Research on Wavelet Based Autofocus Evaluation in Micro-vision

ZONG Guang-hua, SUN Ming-lei, BI Shu-sheng, DONG Dai

(*School of Mechanical Engineering and Automation, Beijing University of Aeronautics and Astronautics, Beijing 100083, China*)

Abstract: This paper presents the construction of two kinds of focusing measure operators defined in wavelet domain. One mechanism is that the Discrete Wavelet Transform (DWT) coefficients in high frequency subbands of in-focused image are higher than those of defocused one. The other mechanism is that the autocorrelation of an in-focused image filtered through Continuous Wavelet Transform (CWT) gives a sharper profile than blurred one does. Wavelet base, scaling factor and form to get the sum of high frequency energy are the key factors in constructing the operator. Two new focus measure operators are defined through the autofocusing experiments on the micro-vision system of the workcell for micro-alignment. The performances of two operators can be quantificationally evaluated through the comparison with two spatial domain operators—Brenner Function (BF) and Squared Gradient Function (SGF). The focus resolution of the optimized DWT-based operators is 14% higher than that of BF and its computational cost is 52% approximately lower than BF's. The focus resolution of the optimized CWT-based operators is 41% lower than that of SGF whereas its computational cost is approximately 36% lower than SGF's. It shows that the wavelet based autofocus measure functions can be practically used in micro-vision applications.

Key words： vision；image analysis；autofocus；wavelet；autocorrelation；focus measure

显微视觉自动聚焦的小波测度研究. 宗光华，孙明磊，毕树生，董代. 中国航空学报(英文版), 2006, 19(3): 239-246.

摘　要： 离散小波变换(DWT)或连续小波变换(CWT)滤波后自相关运算均可对显微图像中的高频信息进行提取，依据高频能量的大小可以判断图像目标特征的离焦程度。基于上述原理，提出与小波变换相关的两类聚焦测度函数：基于 DWT 的聚焦函数、基于 CWT 滤波后自相关运算的聚焦函数。以 MEMS 器件微对准封装系统中的显微视觉单元作为实验平台，运用实验的方法确定小波基、小波因子以及小波系数的计算形式，得到可用于本显微视觉系统的两个基于小波的聚焦测度：Haar 二级小波分解系数平方和函数；尺度因子为 2^{-5} 的 Mexican-Hat 小波滤波后自相关平方积分函数。最后利用聚焦分辨率与函数计算时间两个参数对聚焦测度函数进行量化评估。与 Brenner 函数及平方梯度函数等聚焦效果较好的基于空域聚焦测度相比：DWT 函数的聚焦分辨率为 8.43，比 Brenner 函数高 14%，其计算时间为 0.61 s，比 Brenner 函数缩短 52%；而 CWT 自相关函数在聚焦分辨率上比平方梯度函数低 41%，但计算时间比平方梯度函数缩短 36%。表明基于小波域的自动聚焦测度函数具有实用价值。

关键词： 视觉；图像分析；自动聚焦；小波；自相关；聚焦测度

文章编号： 1000-9361(2006)03-0239-08　　**中图分类号：** TP242.6^{+}2　　**文献标识码：** A

Higher resolution may be required by some microassembly or analysis tasks, such as hybrid MEMS fabrication, autonomous micro-robotic cell manipulation, fluorescence nuclei analysis and automatic semiconductor mask/wafer alignment[1,2]. In order to achieve high resolution, higher resolu-

Received date：2005-03-25；Revision received date：2005-12-22

Foundation item：Hi-Tech Research and Development Program of China（2002AA404460，2004AA404260）；National “15”,“211 Project” of China

tion microscope optics, which leads to low Depth of Field (DOF), can be used in such case. Autofocus techniques can be used to find automatically the optimum focus position for small DOF. Focusing mechanism plays vital role in the machine vision based Microassembly system. The vision system for high resolution and throughout is essentially useless without an autofocus capability[3].

In the literatures, many autofocus algorithms have been proposed and compared for use in optical microscopic vision. These focus functions can be classified into two groups: function based on (1) spatial domain and function based on (2) frequency domain. Following the literatures[4,5], focus measure operator base on frequency domain can not be used to produce fast algorithms for the computation complexity. Nevertheless, with development of Very Large Scale Integration (VLSI) and Application-Specific Integrated Circuits (ASIC) techniques, the algorithm constructed in frequency domain can be realized in hardware to achieve real-time processing of 2D images[6].

This paper presents an application of the wavelet analysis tool under the scale-space framework. Some focus measure operators based on Discrete Wavelet Transformation (DWT) are constructed in the wavelet transform domain. Another application of Continuous Wavelet Transform (CWT) in constructing focus measure is also reported. A CWT-based focus measure operator is defined under the combination of CWT filter and autocorrelation. All kinds of the operators have been realized in micro-vision sub-system of an automatic microassembly workcell for Polymethylmethacrylate (PMMA) microfluidic chip packaging, which shows better performance than some well proposed spatial domain based focus functions.

1 DWT-Based Autofocus Functions

1.1 Problem and model description

It has been deduced that a well-focused image contains more details than a defocused image from Fourier optics. Most of the focus criteria measure high frequency contents of an image as a measure of focus degree. Although the autofocus is a long standing topic in literatures, no such a generally applicable solution is available. Methods are often designed for one kind of imaging mode. Wavelets were first shown to be the foundation of a powerful new approach to signal processing and analysis called multi-resolution theory[7]. Multi-resolution theory incorporates and unifies techniques from a variety of disciplines, including subband coding from signal processing and pyramidal image processing.

According to Mallat's multi-resolution theory[7], as shown in Fig.1, the 2D original input image $I(x, y)$ is processed by the 2D filters H_{LL}, H_{HL}, H_{LH} and H_{HH} and then subsampled by 2 in each dimension, i.e., overall subsampled by 4. As the result, $I(x, y)$ is divided into four subband images W_{LL_1}, W_{HL_1}, W_{LH_1} and W_{HH_1}. The subbands W_{HL_1}, W_{LH_1} and W_{HH_1} represent the scale wavelet coefficients. To obtain the next coarser scales of wavelet coefficients, the subband W_{LL_1} is further processed and subsampled. The process continues until some final scale N is reached, and $3N+1$ subband images consisting of the Multiresolution Approximation (MRA) component W_{LLn} and the Multiresolution Representation (MRR) components W_{HLn}, W_{LHn} and W_{HHn} are acquired. Fig.1 shows the wavelet decomposition for the scale N=2.

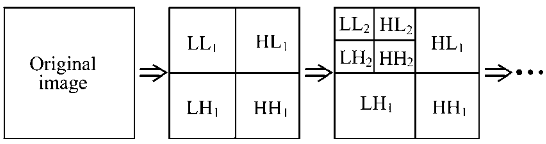

Fig.1 Wavelet packet decomposition for an image

As shown in Fig.2, the testing image sequence used is taken from the micro-vision system of a mi-

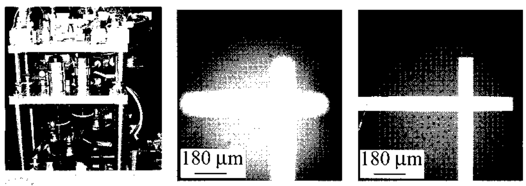

(a)vision system (b)defocused image (c)in-focused image

Fig.2 Experimental setup

croassembly workcell. The image is in the bright-field with cross-shaped feature. A digital CCD camera is used in the imaging unit (A302f of Basler Co.) with matching lenses. All images are captured by the digital camera and are transferred to the host computer through the 1394/PCI adapter (Meteor-Ⅱ/1394 of Matrox Co.). The lenses (zoom 70× of Optem Co.) consist of a right-angle TV-tube adapter, a motorizing 0.75×～5.2× zoom module, a motorizing 3 mm focus module, and a 10×/0.28 microscopic objective (M Plan Apo of Mituoyo Co.). The optical system can achieve significantly higher magnification of 3.6×～25.3×. Taking the N.A. of the 0.28 Mitutoyo objective into consideration, the optical system can resolve 0.6 micron max. The minimum focus motion of the micro-vision system can reach 0.2 micron/step.

A defocused image and an in-focused image are decomposed in level-1 by the DWT filters (Haar basis function) respectively and there are W_{HL_1} and W_{LH_1} of defocused and focused images respectively. As shown in Fig.3, the horizontal detail subband W_{HL_1} and the vertical detail subband W_{LH_1} of focused image contain more energies than that of the defocused image.

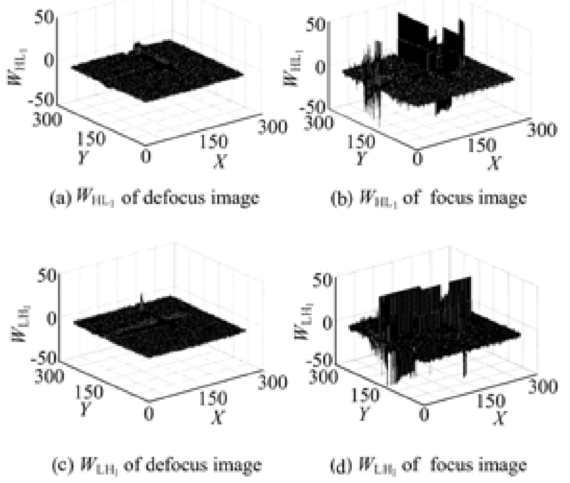

Fig.3 Comparison of high frequency subbands between defocused and in-focused images

1.2 DWT-based focusing measure operators

Three basic DWT-based focus measure operators $F^1_{\mathrm{DWT\_2}^n}$, $F^2_{\mathrm{DWT\_2}^n}$ and $F^3_{\mathrm{DWT\_2}^n}$ are defined as follows,

$$F^1_{\mathrm{DWT\_2}^n}=\sum_{i=1}^{M}\sum_{j=1}^{N}\left|w_{\mathrm{HL}_n}(i,j)\right| \tag{1}$$

$$F^2_{\mathrm{DWT\_2}^n}=\sum_{i=1}^{M}\sum_{j=1}^{N}\left|w_{\mathrm{LH}_n}(i,j)\right| \tag{2}$$

$$F^3_{\mathrm{DWT\_2}^n}=\sum_{i=1}^{M}\sum_{j=1}^{N}\left|w_{\mathrm{HH}_n}(i,j)\right| \tag{3}$$

where DWT_2^n means the wavelet basis and level-n decomposition chosen to acquire subbands, which are necessary for constructing the focus measures. The discrete wavelet transformed images in the level-n LH, HL and HH subbands are denoted W_{HL_n}, W_{LH_n} and W_{HH_n} respectively. W_{HH_n} donates diagonal detail subband.

A sequence of 24 images is captured consecutively at increments of 10 micron as the microscope objective is moved towards the sample. The focusing performance of $F^1_{\mathrm{Haar\_2}^1}$ is compared with those of $F^2_{\mathrm{Haar\_2}^1}$ and $F^3_{\mathrm{Haar\_2}^1}$ using the image sequence. Note that an ideal autofocus curve should reach a single sharp maximum at the focal position and decay monotonically both above and below the optimal focal position[1]. Three focus measure curves are shown in Fig.4. The data for each curve are scaled (normalized) so that all maxima are unity. It can be observed that the curves of $F^1_{\mathrm{Haar\_2}^1}$ and $F^2_{\mathrm{Haar\_2}^1}$ can reach a single sharp maximum at the focal position, but they can not give the strictly monotonical profile on both sides of the focal position.

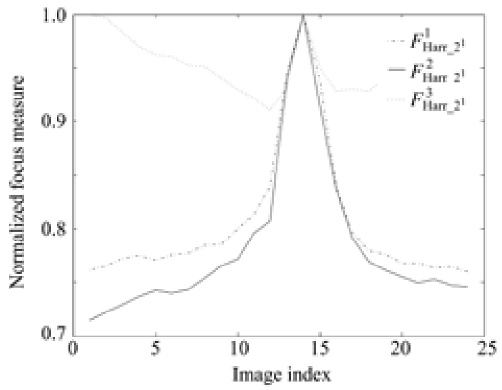

Fig.4 Performance comparison of $F^2_{\mathrm{Haar\_2}^1}$, $F^2_{\mathrm{Haar\_2}^1}$ and $F^3_{\mathrm{Haar\_2}^1}$

Another DWT-based focus measure operator is given to improve the above Eq.(1), Eq.(2) and Eq.(3),

$$F^4_{\mathrm{DWT}\_2^n} = \sum_{i=1}^{M}\sum_{j=1}^{N}\left[\left|w_{\mathrm{HL}_n}(i,j)\right| + \left|w_{\mathrm{LH}_n}(i,j)\right|\right]^2 \qquad (4)$$

As shown in Fig.5, the focus performance of $F^4_{\mathrm{Haar}\_2^1}$ is compared with $F^1_{\mathrm{Haar}\_2^1}$ and $F^2_{\mathrm{Haar}\_2^1}$ using the image sequence. It can be observed that $F^4_{\mathrm{Haar}\_2^1}$ gives the sharpest focus measure profile, and more important, the curve of $F^4_{\mathrm{Haar}\_2^1}$ ascends monotonically with the increasing focal position on left side of focal position and decays monotonically with increasing focal position on right side of focal position.

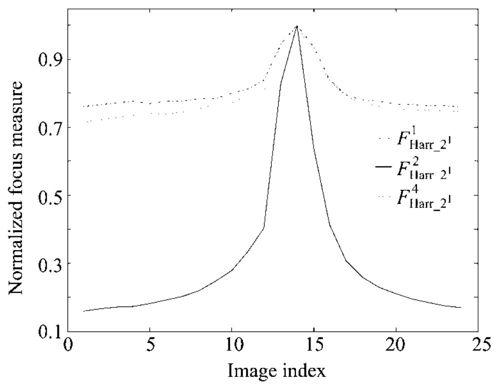

Fig.5 Performance comparison of $F^1_{\mathrm{Haar}\_2^1}$, $F^2_{\mathrm{Haar}\_2^1}$ and $F^4_{\mathrm{Haar}\_2^1}$

The performance of $F^4_{\mathrm{Haar}\_2^1}$ is superior to those that of $F^1_{\mathrm{Haar}\_2^1}$, $F^2_{\mathrm{Haar}\_2^1}$ and $F^3_{\mathrm{Haar}\_2^1}$.

Wavelet-based operators are flexible in that they can be used with different wavelet bases optimized for different applications[7]. Selection of wavelet bases is an important feature of the DWT-based focus measure operator construction. Some commonly used symmetry wavelet bases Haar, Coiflets, Daubechies and Dmey are chosen to construct focus measure operators. As shown in Fig.6, the performance of $F^4_{\mathrm{Haar}\_2^1}$ is compared with those of $F^4_{\mathrm{DB2}\_2^1}$, $F^4_{\mathrm{DB4}\_2^1}$, $F^4_{\mathrm{DB6}\_2^1}$, $F^4_{\mathrm{Coif}\_2^1}$ and $F^4_{\mathrm{Dmey}\_2^1}$. It can be observed that the focus curve of $F^4_{\mathrm{Haar}\_2^1}$ gives the sharper and more strictly monotonical focus measure profile than those of others in far-focus positions. So Haar base is more suitable than other wavelet bases in focus measure operator construction.

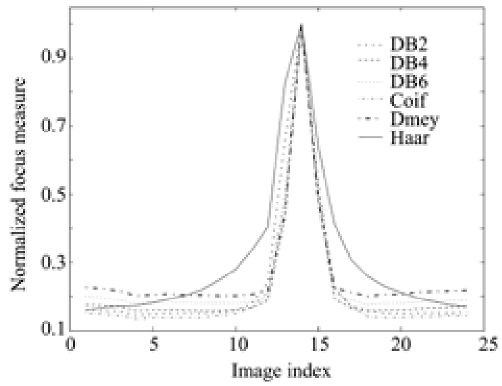

Fig.6 Performance comparison of $F^4_{\mathrm{DB2}\_2^1}$, $F^4_{\mathrm{DB4}\_2^1}$ $F^4_{\mathrm{DB6}\_2^1}$, $F^4_{\mathrm{Coif}\_2^1}$, $F^4_{\mathrm{Dmey}\_2^1}$ and $F^4_{\mathrm{Haar}\_2^1}$

In addition to the selection of wavelet bases, the selection of wavelet decomposition scale level is another important feature of the DWT-based focus measure operator construction. As shown in Fig.(7), the performance of $F^4_{\mathrm{Haar}\_2^2}$ is compared with those of $F^4_{\mathrm{Haar}\_2^1}$, $F^4_{\mathrm{Haar}\_2^3}$ $F^4_{\mathrm{Haar}\_2^4}$, $F^4_{\mathrm{Haar}\_2^5}$ and $F^4_{\mathrm{Haar}\_2^6}$. $F^4_{\mathrm{Haar}\_2^n}$ means the operator contructed with *Haar* wavelet and 2^n resolution level in DWT domain. It can be observed that $F^4_{\mathrm{Haar}\_2^2}$ gives the sharper and more strictly monotonical focus measure profile than others in far-focus positions. Then the optimized focus measure operator $F^4_{\mathrm{Haar}\_2^2}$ can be given by

$$F^4_{\mathrm{Haar}\_2^2} = \sum_{i=1}^{M}\sum_{j=1}^{N}\left[\left|w_{\mathrm{HL}_2}(i,j)\right| + \left|w_{\mathrm{LH}_2}(i,j)\right|\right]^2 \qquad (5)$$

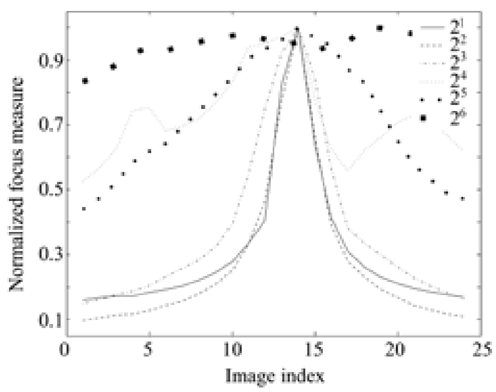

Fig.7 Performance comparison of $F^4_{\mathrm{Haar}\_2^1}$, $F^4_{\mathrm{Haar}\_2^2}$, $F^4_{\mathrm{Haar}\_2^3}$, $F^4_{\mathrm{Haar}\_2^4}$, $F^4_{\mathrm{Haar}\_2^5}$ and $F^4_{\mathrm{Haar}\_2^6}$

2 CWT and ACT-Based Autofocus Functions

2.1 Problem and model description

Autocorrelation Transform (ACT) is the basic statistical approach to be used for measuring the degree of edge variation in images. So this technique based on contrast measurement can also be used in autofocusing algorithm. The autocorrelation of an in-focused image gives a sharper correlation peak than that of a defocused image.

The autocorrelation transform measure can be given by

$$F_{\mathrm{ACT}} = \sum_{\varepsilon=1}^{N} \left| C_{\mathrm{ACT}}(\varepsilon) \right| \tag{6}$$

where $C_{\mathrm{ACT}}(\varepsilon)$ can be represented as

$$C_{\mathrm{ACT}}(\varepsilon) = \sum_{i=1}^{M} \left[f(i+\varepsilon) \cdot f(i) \right] \Big/ \sum_{i=1}^{M} \left[f(i) \right]^2$$

The 1-D cross-sectional scans of in-focused, slightly defocused and acutely defocused testing images taken by vision system (Fig.2) are used to measure the degree of focus. As shown in Fig.8, the acutely defocused scene has more width curve than other two curves do. But the autocorrelation curves of slight defocused and in-focused images can hardly be identified. The conventional autocorrelation technique may cause inaccuracy because the widths of autocorrelation curves in near-focus region are approximately the same.

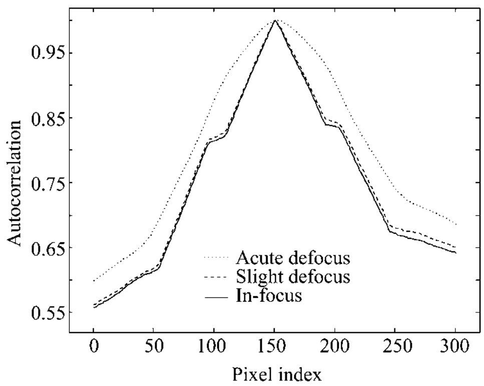

Fig.8 Autocorrelation computations between acutely defocused, slight defocused and in-focused image

Continuous Wavelet Transform (CWT) filter can be used to enhance the edge feature (high frequency information) of image before autocorrelation computation is conducted[8,9]. As shown in Fig.9, 1-D testing image signals are filtered by Mexican-Hat wavelet with 2^{-2} scale factor first, and then autocorrelation computation is conducted. It can be observed that the autocorrelation profiles of slightly defocused and in-focused image signals can be easily identified after appropriate CWT.

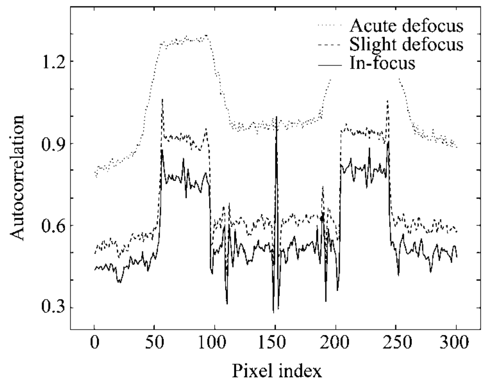

Fig.9 Autocorrelation computations between Mexican-Hat wavelet (2^{-2} scale) transformed acutely defocused, slightly defocused and in-focused image

Continuous wavelet processing filters with different wavelet bases may cause different effects in defocus degree measurement. As shown in Fig.9 and Fig.10, autocorrelation curves of the 1-D testing image signals filtered by Meyer wavelet with 2^{-2} scale factor are brought into comparison with curves of signals filtered by Mexican-Hat wavelet with the same scale factor. It can also be ease to identify the autocorrelation curves of slightly defocused and in-focused, but the Mexican-Hat wavelet filter brings better high frequency enhancement effect than the Meyer wavelet does in processing the testing images given.

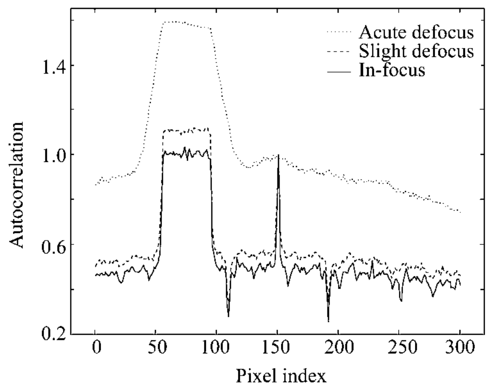

Fig.10 Autocorrelation computations between Meyer wavelet (2^{-2} scale) transformed acutely defocused, slightly defocused and in-focused image

CWT-based filters with different scale factors may also cause different effects in defocus degree measurement. As shown in Fig.10 and Fig.11, the autocorrelation curves of 1-D testing image signals filtered by Meyer wavelet with 2^{-2} scale factor are brought into comparison with curves of signals filtered by the same wavelet with different scale factor 2^4. It can be seen from the Fig.11 that the autocorrelation curves of slightly the defocused image and the in-focused image are approximately the same.

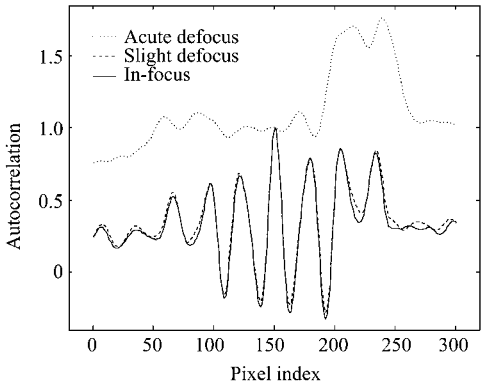

Fig.11 Autocorrelation computations between Meyer wavelet (2^4 scale) transformed acutely defocused, slightly defocused and in-focused image

2.2 CWT and ACT-based focusing measure ope-rators

A concision CWT and ACT-based focus measure operator $F^1_{\mathrm{CWT}\_2^n}$ is defined as follows,

$$F^1_{\mathrm{CWT}\_2^n} = \sum_{\varepsilon=1}^{N} \left| C_{\mathrm{W}}(\varepsilon) \right| \tag{7}$$

where $C_{\mathrm{W}}(\varepsilon)$ can be represented as

$$C_{\mathrm{W}}(\varepsilon) = \sum_{\tau=1}^{M} \left[W_f(s,\tau+\varepsilon) \cdot W_f(s,\tau) \right] \Big/ \sum_{\tau=1}^{M} \left[W_f(s,\tau) \right]^2$$

$$W_f(s,\tau) = \left\langle f, \psi_{s,\tau} \right\rangle = \frac{1}{\sqrt{|a|}} \int_{\Re} f(t) \cdot \psi^* \left(\frac{t-\tau}{s} \right) \mathrm{d}t$$

here, $W_f(s,\tau)$ represents the continuous wavelet transform of $f(i) \in L^2(R)$. τ is the translation factor; s is the scale factor. $C_{\mathrm{W}}(\varepsilon)$ donates autocorrelation computation in CWT domain.

The testing sequence of 24 images mentioned is first used to compare focus measure the performance of Eq.(6) with that of Eq.(7). As shown in Fig.12, three focus measure curves are shown, and the focus performance of conventional autocorrelation-based F_{ACT} is compared with those of CWT and ACT-based $F^1_{Meyer\_2^{-2}}$ and $F^1_{M-H\_2^{-2}}$. It can be observed that $F^1_{Meyer\_2^{-2}}$ and $F^1_{M-H\_2^{-2}}$ reach a single sharp maximum at focal position, but F_{ACT} can not. This proves that the CWT-based filter technique can improve the autofocus inaccuracy caused by conventional ACT-based measure.

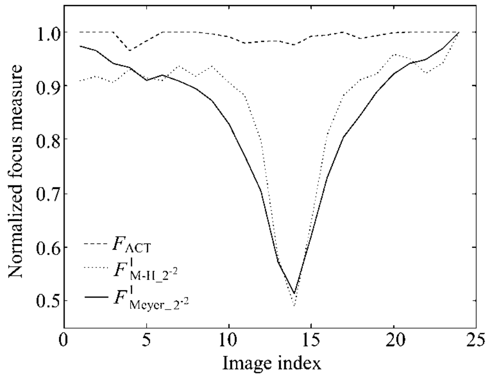

Fig.12 Performance comparisons of F_{ACT}, $F^1_{\mathrm{M-H\_2^{-2}}}$ and $F^1_{\mathrm{Meyer\_2^{-2}}}$

Note that different scaling factors must be optimized for images with different features. Mexican-Hat wavelet filter with scaling factors from 2^{-5} to 2^8 are conducted in focus measure algorithm. Fig.13 and Fig.14 show that the focus measure performance improvements become much more significant when $s > 2^{-5}$, where s means the scaling factor.

For further improving the focus measure performance of Eq.(7), another operator is given by

$$F^2_{\mathrm{CWT}\_2^n} = \sum_{\varepsilon=1}^{N} \left[C_{\mathrm{W}}(\varepsilon) \right]^2 \tag{8}$$

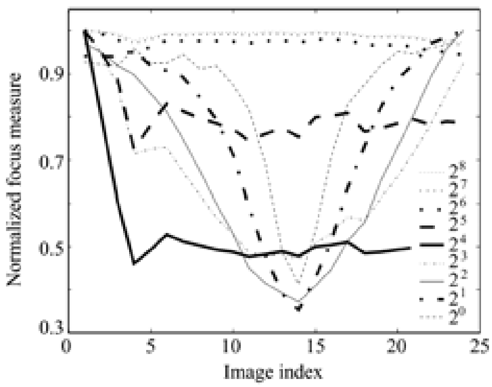

Fig.13 Performance comparisons of $F^1_{M-H\_2^n}$ with scaling factor from 2^0 to 2^8

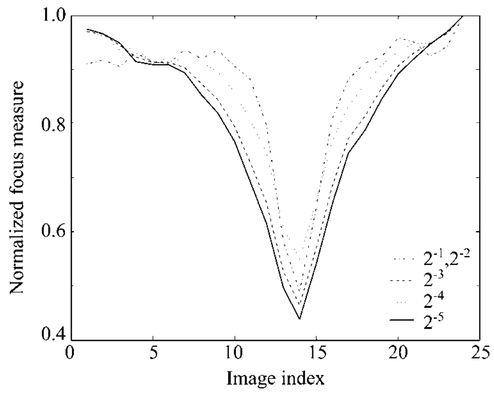

Fig.14 Performance comparisons of $F^{1}_{M-H\_2^{n}}$ with scaling factor from 2^{-5} to 2^{-1}

It can be seen from Fig.15 that the experimental curve width of $F^{2}_{\mathrm{M-H\_2^{-2}}}$ is sharper than that of $F^{1}_{\mathrm{M-H\_2^{-2}}}$.

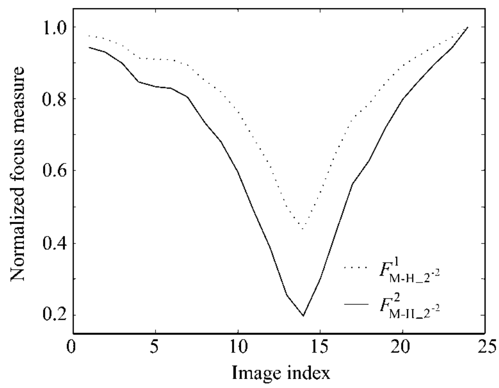

Fig.15 Performance comparison of $F^{1}_{\mathrm{M-H\_2^{-2}}}$ and $F^{2}_{\mathrm{M-H\_2^{-2}}}$

3 Quantitative Evaluation

Varieties of focus measure operators based on spatial domain have been proposed[10,11]. Two classic operators, Brenner function (Eq.(9)) and sum of squared gradient function (Eq.(10)) were reported to be the most effective. So a DWT-based focus measure operator $F^{4}_{\mathrm{Haar\_2^{2}}}$ (Eq.(11)) and a CWT and ACT-based operator $F^{2}_{\mathrm{M-H\_2^{-5}}}$ (Eq.(12)) are constructed to compare to those two spatial domain based operators through quantitative evaluation.

The normalized focus curves of the following measures are shown in Fig.16.

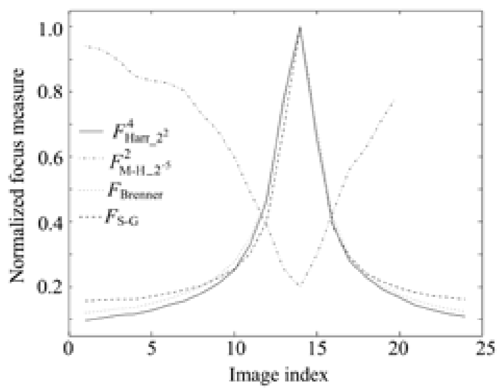

Fig.16 Performance comparisons of $F^{4}_{\mathrm{Haar\_2^{2}}}$, $F^{2}_{\mathrm{M-H\_2^{-5}}}$, F_{Brenner} and $F_{\mathrm{S-G}}$

(1) Brenner function[11]

$$F_{\mathrm{Brenner}}=\sum_{i=1}^{512}\sum_{j=1}^{510}\left[f(i,j+2)-f(i,j)\right]^{2} \tag{9}$$

(2) Sum of squared gradient function[10]

$$F_{\mathrm{S-G}}=\sum_{i=1}^{511}\sum_{j=1}^{511}\left\{\left[f(i,j+1)-f(i,j)\right]^{2}+\left[f(i+1,j)-f(i,j)\right]^{2}\right\} \tag{10}$$

(3) DWT-based operator

$$F^{4}_{\mathrm{Haar\_2^{2}}}=\sum_{i=1}^{128}\sum_{j=1}^{128}\left[\left|w_{\mathrm{HL_2}}(i,j)\right|+\left|w_{\mathrm{LH_2}}(i,j)\right|\right]^{2} \tag{11}$$

(4) CWT and ACT-based operator

$$F^{2}_{\mathrm{M-H\_2^{-5}}}=\sum_{\varepsilon=1}^{150}\left|C_{\mathrm{W}}(\varepsilon)\right|^{2} \tag{12}$$

Qualitative evaluations of DWT and CWT and ACT based focus operators previously constructed in this paper allow selecting the most appropriate function for the application in a visual and intuitive form. Sometimes qualitative evaluation is important, but sometimes quantitative evaluation is necessary to give a more detailed study in selection of focus measures. Two features of focus performance are quantificationally evaluated through experiments. One feature is the commonly used execution time t, and the other is the focus resolution σ^2.

According to Heisenberg Uncertain Principle (HUP) and Autofocus Uncertain Measure (AUM)[12], focus resolution can be defined by[13]

$$\sigma^{2}=\frac{1}{\|f\|^{2}}\int_{-\infty}^{+\infty}\left[\left(x-x_{\mathrm{p}}\right)\cdot f(x)\right]^{2}\mathrm{d}\,x$$

The form in discrete domain is given by

$$\sigma^2 = \frac{1}{\|f\|^2}\sum_{i=1}^{n}\left[\left(i-i_p\right)\cdot f\left(i\right)\right]^2 \tag{13}$$

where $f(i)$ donates the computed focus measure operator in position i and i_{p} donates the in-focus position.

The evaluation results of t and σ^2 for focus curves in Fig.16 are listed in Table 1 and Table 2.

Table 1 Computed execution time for Fig.16

Focus measure	F_{Brenner}	$F_{\mathrm{S-G}}$	$F^4_{\mathrm{Haar\_2^2}}$	$F^2_{\mathrm{M-H\_2^{-5}}}$
Window	512×512	512×512	128×128	150×1
t/s	1.27	2.12	0.61	1.36

Table 2 Computed focus resolutions for Fig.16

Focus measure	F_{Brenner}	F_{S-G}	$F^4_{\mathrm{Haar\_2^2}}$	$F^2_{\mathrm{M-H\_2^{-5}}}$
σ^2	8.43	18.79	9.81	13.25

4 Conclusions

Two methods of focus measure operators construction in wavelet domain have been reported. These operators can be optimized according to the selection of wavelet base and scaling factor.

According to qualitative evaluation on experimental focus curves, a DWT-based focus measure operator $F^4_{\mathrm{Haar\_2^2}}$ and a CWT and ACT-based operator $F^2_{\mathrm{M-H\_2^{-5}}}$ are selected. To compare with two well proposed spatial domain operators, the quantitative evaluation is executed.

(1) The focus resolution of $F^4_{\mathrm{Haar\_2^2}}$ is 14% higher than that of F_{Brenner} and the computational cost of $F^4_{\mathrm{Haar\_2^2}}$ is 52% approximately lower than that of F_{Brenner}.

(2) The focus resolution of $F^2_{\mathrm{M-H\_2^{-5}}}$ is 41% lower than that of $F_{\mathrm{S-G}}$ whereas the computational cost of $F^2_{\mathrm{M-H\_2^{-5}}}$ is approximately 36% lower than that of $F_{\mathrm{S-G}}$.

Experimental results show that the wavelet based autofocus measures possess high performance in high-frequency information sensitivity and the techniques can be practically used in micro-vision applications.

References

[1] Allegro S, Chanel C, Jacot J. Autofocus for automated microassembly under a microscope[J]. Image Processing,1996,1:677-680.

[2] Hughlett E, Kaiser P. An autofocus technique for imaging microscope[J]. Acoustics Speech and Signal Processing,1992,3:93-96.

[3] Hughlett E, Cooper K. A video based alignment system for X-ray lithography[C]//SPIE Symposium on Microlithography Processing.1991:1465-1468.

[4] Yeo T, Ong S, Sinniah R. Autofocusing for tissue microscopy[J]. Image Vision Comput,1993,11:629-639.

[5] Santos A, De Solorzano C O, Vaquero J J, et al. Evaluation of autofocus functions in molecular cytogenetic analysis[J]. Journal of Microscopy,1997,188(3):264-272.

[6] Gamadia M, Peddigari V, Kehtarnavaz N, et al. Real-time implementation of autofocus on the TI DSC processor[C]//Proc of SPIE-IS and T Electronic Imaging.2004:10-18.

[7] Mallat S. A theory for multiresolution signal decomposition: the wavelet representation[J]. IEEE Transactions on Pattern Analysis and Machine Intelligence,1989,11(7):674-693.

[8] 黄剑琪,冯华君,徐之海,等. 边缘特征增强算法和小波分析在精确聚焦中的应用[J].光子学报,2000,29(10):932-936.
Huang J Q, Feng H J, Xu Z H, et al. The application of edge-enhance algorithm and wavelet analysis in auto-focus[J]. Acta Photonica Sinica, 2000, 29(10):932-936. (in Chinese)

[9] Widjaja J, Jutamulia S. Wavelet transform-based autofocus camera system[J]. Circuits and Systems, IEEE APCCAS,1998,3:49-51.

[10] Subbarao M, Tyan J. Selecting the optimal measure for autofocusing and depth-from-focus[J]. IEEE Transactions on Pattern Analysis and Machine Intelligence,1998,20(8):
864-870.

[11] Brenner J F, Dew B S, Horton J B，et al. An automated microscope for cytologic research[J]. Cytometry,1971,24:100-111.

[12] Subbarao M, Tyan J K，et al. Selecting the optimal focus measure for autofocusing and depth-from-focus[J]. IEEE Trans of Pattern Analysis and Machine Intelligence,1998,20(8):864-870.

[13] Yang G, Nelson B J. Wavelet-based autofocusing and unsupervised segmentation of microscopic images[C]//Proceedings of the 2003 IEEE/RSJ Int Conference on Intelligent Robots and Systems.2003:2143-2148.

Biography:

ZONG Guang-hua Professor at the School of Mechanical Engineering and Automation, Beijing University of Aeronautics and Astronautics(BUAA). His research interests includes robotics and mechanism. He has published several scientific papers in various periodicals. Tel: (010) 82317749, E-mail: ghzong@buaa.edu.cn

SUN Ming-lei Born in 1974, he received B.S. and M.S. from Beijing University of Aeronautics and Astronautics in 1997 and 2003 respectively, and now studies as a doctor candidate in the Robotics Research Institute of BUAA. Tel: (010) 82338019, E-mail: mingleisun@263.net